THE JOURNAL OF BIOLOGICAL CHEMISTRY VOL. 291, NO. 23, pp. 12119–12125, June 3, 2016

Formation of a Chloride-conducting State in the Maltose ATP-binding Cassette (ABC) Transporter*

Received for publication, December 20, 2015, and in revised form, April 6, 2016 Published, JBC Papers in Press, April 7, 2016, DOI 10.1074/jbc.M115.711622

Michael L. Carlson[1], **Huan Bao**[2], **and Franck Duong**[3]

From the Department of Biochemistry and Molecular Biology, University of British Columbia, Vancouver, British Columbia V6T 1Z3, Canada

ATP-binding cassette transporters use an alternating access mechanism to move substrates across cellular membranes. This mode of transport ensures the selective passage of molecules while preserving membrane impermeability. The crystal structures of $MalFGK_2$, inward- and outward-facing, show that the transporter is sealed against ions and small molecules. It has yet to be determined whether membrane impermeability is maintained when $MalFGK_2$ cycles between these two conformations. Through the use of a mutant that resides in intermediate conformations close to the transition state, we demonstrate that not only is chloride conductance occurring, but also to a degree large enough to compromise cell viability. Introduction of mutations in the periplasmic gate lead to the formation of a channel that is quasi-permanently open. $MalFGK_2$ must therefore stay away from these ion-conducting conformations to preserve the membrane barrier; otherwise, a few mutations that increase access to the ion-conducting states are enough to convert an ATP-binding cassette transporter into a channel.

Most membrane transporters facilitate the movement of substrate molecules using an alternating access mechanism (1–5). This conserved mode of transport corresponds to a cycle of conformational changes coupled to the movement of gating elements or rigid-body structures on either side of the membrane (5–7). This movement results in the alternate exposure of the substrate-binding site to the extracellular and intracellular environments (2, 6). Intermediate states, which normally occur only transiently during transport, lie between the inward- and outward-facing conformations (8, 9).

The alternating access mechanism ensures that the free flow of ions and water molecules is restricted during transport (1, 10). Accordingly, because only one gate is open at a given time, the transporter is switching conformations without ever producing a membrane channel (8). Space-filling models derived from the crystal structures of inward- and outward-facing transporters indicate that the gates are sufficiently tight to prevent the passage of ions and water molecules (2, 7, 11). However, crystal structures represent static conformations. It is therefore unknown whether the dynamics of the gates, especially during conformational transitions, are coordinated enough to prevent the passage of ions and water molecules.

A recent molecular dynamics simulation on various alternating access transporters reported that water passage might be possible through short-lived intermediates states (9). It was proposed that these water-conducting states are inherently characteristic to the alternating access mechanism. Water conductance has also been reported in the family of ion co-transporters (12–14). However, in the ABC[4] transporter family, with the exception of CFTR (15), there is no such evidence. This may be due to the highly transient nature of the intermediate states, which makes detection inherently difficult (9).

In this study, we utilize the $MalFGK_2$ transporter to explore the gating mechanism. The substrate translocation pathway is comprised of two membrane proteins, MalF and MalG. The nucleotide-binding domain, which controls the conformation of MalFG, is composed of the homodimeric MalK subunit. Transport also requires the periplasmic binding protein MalE to traffic maltose to the transporter and to stimulate its ATPase activity (16–18). In this study, to facilitate the detection of ion conduction, we employed the mutant transporter MalF500 (19, 20). This mutant hydrolyzes large amounts of ATP independent from MalE and maltose. This high ATPase activity is due to the mutant resting in intermediate conformations near the transition state (20–22). Our results demonstrate that MalF500 forms an ion-conducting channel that, when overproduced, is deleterious to the cell. In contrast, wild-type $MalFGK_2$ rests in the inward-facing conformation, which is impermeable to ions.

Experimental Procedures

Reagents—The detergent dodecyl maltoside (DDM) was purchased from Anatrace. The lipids 1,2-dioleoyl-*sn*-glycero-3-phosphocholine (DOPC) and 1,2-dioleoyl-*sn*-glycero-3-phospho-1′-*rac*-glycerol (DOPG) and *Escherichia coli* polar lipid extract were purchased from Avanti Polar Lipids. Superdex 200 10/300 GL, Resource 15Q, and nickel-nitrilotriacetic acid-chelating Sepharose columns were obtained from GE Healthcare. All other chemicals were obtained from Sigma. The proteins MalE and $MalFGK_2$ were purified as described previously

* This work is supported by operating grants from the Canadian Institutes of Health Research. The authors declare that they have no conflicts of interest with the contents of this article.

[1] Recipient of a Cellular Dynamics of Macromolecular Complexes NSERC-CREATE scholarship.

[2] Present address: Dept. of Neuroscience, Wisconsin Institute of Medical Research, Madison, WI 53705.

[3] To whom correspondence should be addressed: Dept. of Biochemistry and Molecular Biology, University of British Columbia, 2350 Health Sciences Mall, Vancouver, BC V6T 1Z3, Canada. Tel.: 604-822-5975; Fax: 604-822-522; E-mail: fduong@mail.ubc.ca.

[4] The abbreviations used are: ABC, ATP-binding cassette; DDM, dodecyl maltoside; DOPC, 1,2-dioleoyl-*sn*-glycero-3-phosphocholine; DOPG, 1,2-dioleoyl-*sn*-glycero-3-phospho-1′-*rac*-glycerol; CFTR, cystic fibrosis transmembrane conductance regulator.

(23) using plasmids pBAD33-MalE, pTrc-MalFGK$_2$, and pBAD22-MalFGK$_2$. Cysteine mutations were introduced into MalF (positions Ala-394 and Val-442) and MalG(positions Val-230 and Thr-182) using plasmid pTrc-MalFGK$_2$ as a template. Glycine mutations were introduced into MalF (Val-442) and MalG (Val-230, Thr-228) using plasmid pBAD22-MalFGK$_2$. Mutations were introduced through polymerase incomplete primer extension (24) and verified by sequencing. The plasmids encoding for the SecYEG translocation channel (pBAD22-SecEYG) with deletions in the plug domain (pBAD22-SecEY$_{\Delta 61-70}$G) were described previously (25).

Cysteine Cross-linking—Cross-linking reactions were performed in buffer A (50 mM Tris-HCl (pH 8.0), 100 mM NaCl, 10% glycerol, 5 mM $MgCl_2$, and 0.02% DDM) for 6 min at 37 °C using 5 μM MalFGK$_2$ and 100 μM copper-*O*-phenanthroline ($CuPhe_3$). Reactions were stopped with *N*-ethylmaleimide (5 mM) before analysis by 15% SDS-PAGE. The MalFGK$_2$ complex carrying the cysteine mutations on the periplasmic gate (MalF$_{V442C}$-MalG$_{V230C}$) was reduced with 4 mM dithioerythritol and dialyzed in buffer A plus 40 μM dithioerythritol before cross-linking assays.

Incorporation of Proteins into Proteoliposomes—Total *E. coli* lipids dissolved in chloroform were dried under a stream of nitrogen. The lipids were resuspended in TSG buffer (50 mM Tris-HCl (pH 7.8), 100 mM NaCl, and 10% glycerol) containing 0.5% DDM. The lipids were mixed with the purified MalFGK$_2$ complex at a protein:lipid ratio of 1:2000 in TSG buffer plus 0.1% DDM. Detergent was removed using BioBeads (one-half volume) and gentle shaking overnight at 4 °C. Proteoliposomes were isolated by centrifugation (100,000 × *g*, 1 h, 4 °C) and resuspended in TSG buffer at a final concentration of 3 μM MalFGK$_2$. For incorporation of ergosterol into proteoliposomes, a mixture of DOPC:DOPG: ergosterol (ratio 60:20:20) was dissolved in chloroform, air-dried, and resuspended in S buffer (50 mM HEPES (pH 7.4), NaCl 150 mM, and 0.5% DDM) before addition of MalFGK$_2$. To incorporate nystatin, proteoliposomes were first frozen in liquid N_2, after which they were thawed on ice in the presence of nystatin (75 μg/ml) and then briefly sonicated (15 s, three times) (26).

Spheroplast Membrane Permeability Assays—E. coli strain KM9 (*unc*−) was transformed with pBAD-MalFGK$_2$ or pBAD-SecEYG. Cells were grown in LB medium to OD_{600} ~0.4 before induction with 0.2% arabinose. Cells were harvested 60 min after induction (3000 × *g*, 10 min), washed with 1 volume of 5% sucrose buffer (20 mM Tris-SO_4 (pH 7.8)), and resuspended in 1/20 cell culture volume of 18% sucrose buffer. Cells were converted to spheroplasts by addition of 0.1 mg/ml lysozyme and 2 mM EDTA for 10 min on ice. Conversion to spheroplasts was considered complete when cell lysis was total and immediate upon dilution into water. To measure membrane permeability, spheroplasts were diluted 20-fold in 500 μl of buffer L (293 mM KCl and 20 mM Tris-SO_4 (pH 7.8)) in the presence or absence of valinomycin (5 μM). Cell lysis was measured every 5 s at 540 nm. Tips with a large diameter were employed at all times to prevent pressure-induced lysis during pipetting.

Planar Lipid Bilayer Experiments—The electrical currents were recorded on a planar lipid bilayer work station (BLM, Warner Instruments) composed of a Digidata 1440 low-noise data acquisition system and a BC-535 bilayer clamp amplifier. Unless otherwise stated, the recorded data were sampled at 1 kHz. The lipid bilayers were painted across a 150-μm hole aperture using a flame-smoothed glass applicator stick dipped into a mixture of DOPC:DOPG (ratio 70:30 at 15 mg/ml) in hexadecane. Lipid bilayers were considered ready for protein insertion when their capacitance reached 70–90 picofarad. The chambers on the *cis* side and *trans* side of the bilayer were adjusted to 650 mM KCl and 150 mM KCl, respectively. The two chambers were connected to Ag/$AgCl_2$ electrodes using an agarose salt bridge (2% agarose in 1 M KCl). The electrical current across the lipid bilayer was stable for at least 10 min before addition of proteoliposomes in the *cis* chamber. Fusion of the proteoliposomes to the lipid bilayer was facilitated using a stirring magnet. The bilayers containing channel activity were sometimes broken but could be repainted from the *cis* chamber. All bilayer measurements were performed at room temperature. Data were recorded and analyzed using the Axoclamp pClamp software suite, version 10.2.

Other Methods—The ATPase activity of the maltose transporter was determined by measuring the release of inorganic phosphate using the malachite green photocolorimetric method (27). Protein concentrations were determined using the Bradford assay (28).

Results

MalF500 Can Readily Access the Transition State—In the absence of nucleotide, the conformation of the maltose transporter is inward-facing (6, 18). The transporter becomes outward-facing upon binding of ATP (29). Its basal ATPase activity is also stimulated by MalE and maltose. In contrast, the ATPase activity of MalF500 (bearing mutations MalF$_{N505I}$ and MalG$_{G338R}$) is very high and independent of MalE and maltose (19, 20, 30). It is proposed that mutations in MalF500 destabilize the inward-facing state, thereby diminishing the energy barrier of the transition state (6). To assess the conformation of MalF500, we performed a cross-linking analysis using the cysteine pairs MalF$_{442C}$-MalG$_{230C}$ and MalF$_{394C}$-MalG$_{182C}$ (18, 29). The cysteine pair MalF$_{442C}$-MalG$_{230C}$ reports on the inward-facing conformation of the transporter (Fig. 1*a*). Without ATP, wild-type MalFGK$_2$ is inward-facing, and the cross-link efficiency is maximal (taken as 100%; Fig. 1*b*, *top panel*). In the presence of ATP, MalFGK$_2$ converts to outward-facing, and the cross-link efficiency diminishes to ~43%. The same analysis shows that MalF500 does not depend on ATP because its conformation remains essentially unchanged. Also, the maximal cross-link efficiency is 4-fold lower than that of the wild type (*i.e.* ~20–25%). Thus, MalF500 is resting in a conformation different from inward-facing. We next employed the cysteine pair MalF$_{394C}$-MalG$_{182C,}$ which reports on the outward-facing state of the transporter (Fig. 1*a*). With MalFGK$_2$, the cross-link efficiency is low because the transporter is inward-facing (Fig. 1*b*, *bottom panel*). In the presence of ATP, the cross-link efficiency increases up to ~84% because the transporter becomes outward-facing. In contrast, the cross-link efficiency with MalF500 is maximal, and this conformational change is independent from ATP. Together, these data show that (i) MalF500 rests in a conformation away from the resting state and (ii) that

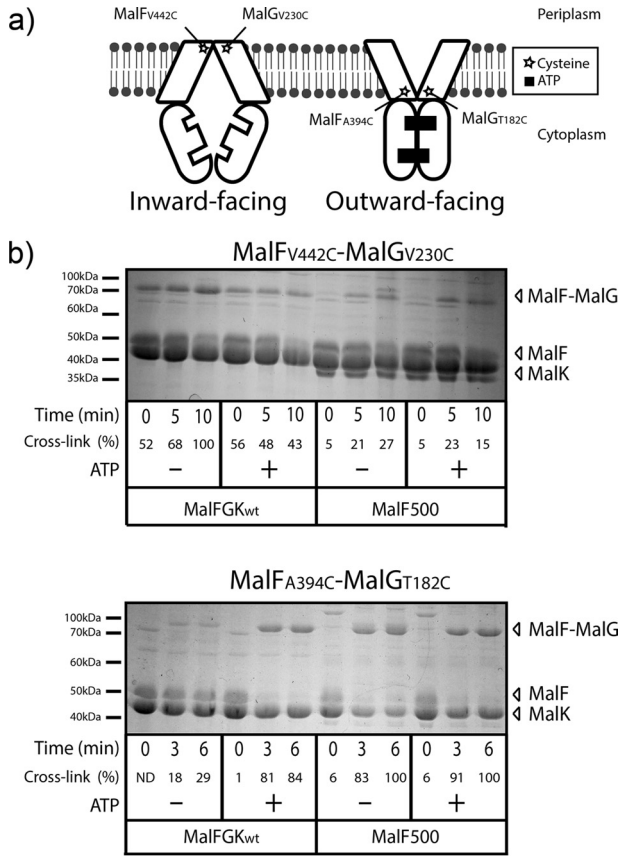

FIGURE 1. **Conformation of MalF500.** *a*, the disulfide bond between MalF$_{V442C}$ and MalG$_{V230C}$ (*stars*) indicates that the transporter is inward-facing. The disulfide bond between MalF$_{A394C}$ and MalG$_{T182C}$ indicates that the transporter is outward-facing. *b*, the MalFGK$_2$ complex in proteoliposome (4.5 μM) was treated with CuPhe$_3$ (100 μM) with or without ATP (2 mM), followed by addition of *N*-ethylmaleimide (5 mM) at the indicated time. The MalF-MalG cross-link products were detected by SDS-PAGE (15%) and Coomassie Blue staining. The cross-link intensity was quantified using ImageJ. The cross-link efficiency of MalFGK$_2$ (V230C-V442C) without ATP is taken as reference point (100%) in the *top panel*. The cross-link efficiency of MalF500 (T182C-A394C) with ATP is taken as reference point (100%) in the *bottom panel*. Each cross-link experiment was repeated at least three times.

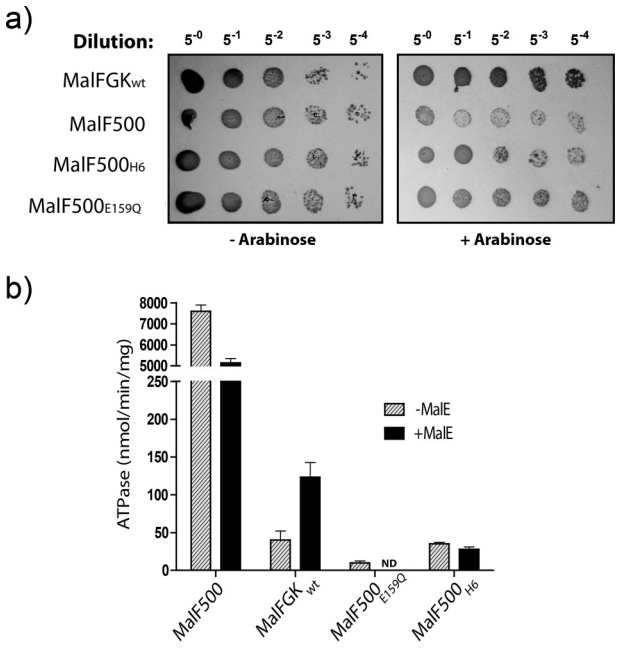

FIGURE 2. **Activity of MalF500.** *a*, effect of MalF500 on cell growth. *E. coli* BL21 was transformed with pBAD22-derived plasmids containing the MalFGK$_2$ complex under control of the arabinose promoter. Cells were grown in LB medium to $OD_{600\,nm}$ ~1.0, serial-diluted, and plated on an LB-agar plate in the presence of 0.02% arabinose to induce expression of the MalFGK$_2$ complex. Plates were incubated at 37 °C for 16 h. *b*, ATPase activity. Proteoliposomes (0.5 μM) and maltose (1 mM) were incubated at 37 °C in the presence or absence of MalE (1 μM) as indicated. Standard deviation was obtained from three separate experiments. *ND*, not detected.

MalF500 reaches the outward-facing conformation independent from ATP. These results explain why MalF500 can easily access the transition state and hydrolyzes larger amounts of ATP in the absence of MalE and maltose.

MalF500 Is Deleterious to the Cell—Overproduction of MalF500 in the membrane results in a significant growth delay (Fig. 2*a*). This may be caused by the high basal ATPase activity of MalF500. It is also possible that the inherent conformational flexibility of MalF500 may increase membrane permeability and compromise cell viability. In an attempt to differentiate the possibilities, we introduced the mutation E159Q into the Walker A motif of MalK (30). This mutation almost fully abolishes ATP hydrolysis (Fig. 2*b*), but the growth of MalF500$_{E159Q}$ is still impaired compared with the wild type (Fig. 2*a*). We then introduced a His$_6$ tag at the N terminus of MalF. The His$_6$ tag decreases the ATPase activity of the wild-type complex through stabilization of the inward-facing conformation (18). Addition of the His$_6$ tag on MalF500 reduces its ATPase activity to wild-type levels (Fig. 2*b*), but the mutant still displays a significant growth defect. These results suggest that the conformation of MalF500, not just its high basal ATPase activity, is detrimental to the cell.

MalF500 Is Permeable to Chloride—We employed a spheroplast lysis assay to determine whether MalF500 affects cell membrane permeability. This method has been developed to study the ion conductance of the SecYEG protein translocation channel (31). Briefly, spheroplasts were diluted into an iso-osmotic solution of KCl in the presence of the K^+ ionophore valinomycin. If the membrane is permeable to Cl^-, the spheroplasts swell and eventually lyse because of the rapid influx of water. As expected, a low degree of lysis was observed in the absence of valinomycin (Fig. 3*a*). In the presence of valinomycin, spheroplasts containing the MalF500 complex lysed immediately (Fig. 3*b*, *red trace*). The initial lysis rate is very high, more than 7-fold higher than spheroplasts containing wild-type MalFGK$_2$ complex and nearly half that of spheroplasts containing the SecYEG channel with an altered plug domain (SecEY$_{\Delta 61-70}$G; Fig. 3*b*, *purple trace*). When the experiment is performed with the mutant MalF500$_{His6}$, the rate of lysis is diminished by ~50% (Fig. 3*b*, *orange trace*). This is consistent with the observation above that a His$_6$ tag at the N terminus of MalF only partially restores cell viability.

Ion Channel Activity of MalF500—The MalF500 complex was purified and incorporated into planar lipid bilayers to determine its ion conductance properties (Fig. 4*a*). The data show that MalF500 has a channel-like activity, and distinct single channel opening and closing events can be resolved. Quantitative analysis of the recordings (Fig. 4, *b* and *c*) further shows that (i) MalF500 creates a membrane channel that is voltage-

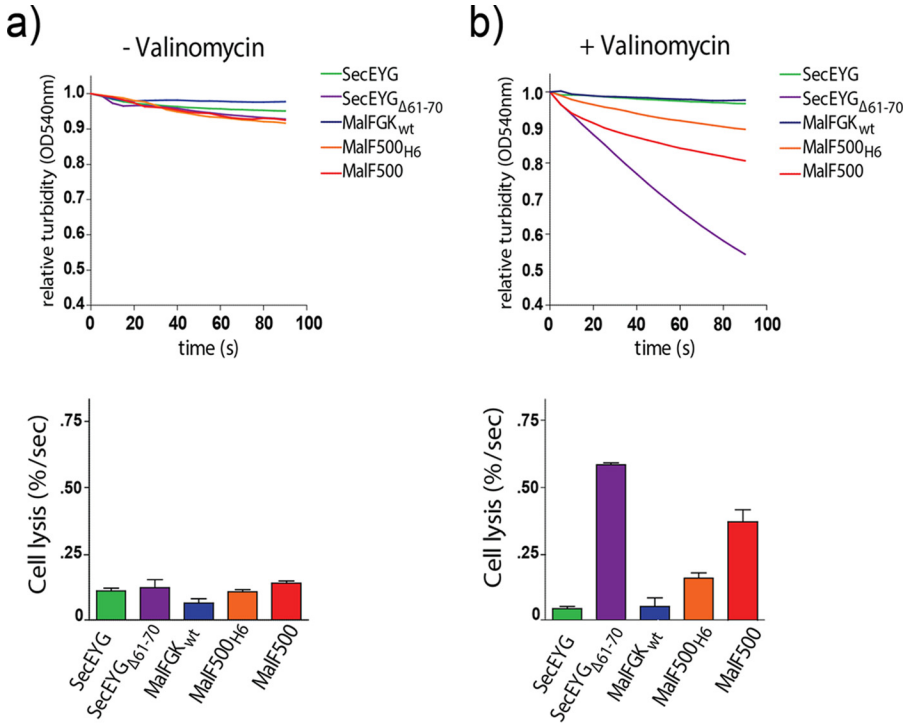

FIGURE 3. **Permeability of MalF500 in spheroplast assays.** *a* and *b*, *E. coli* KM9 (*unc*-) overproducing the indicated complex was converted to spheroplasts and then diluted into an iso-osmotic solution of KCl (293 mM) in the absence (*a*) or presence (*b*) of valinomycin (15 μM). Cell lysis was monitored every 5 s at 540 nm. The rate of lysis is determined from the linear part of the curve (*i.e.* first 30 s after dilution in KCl).

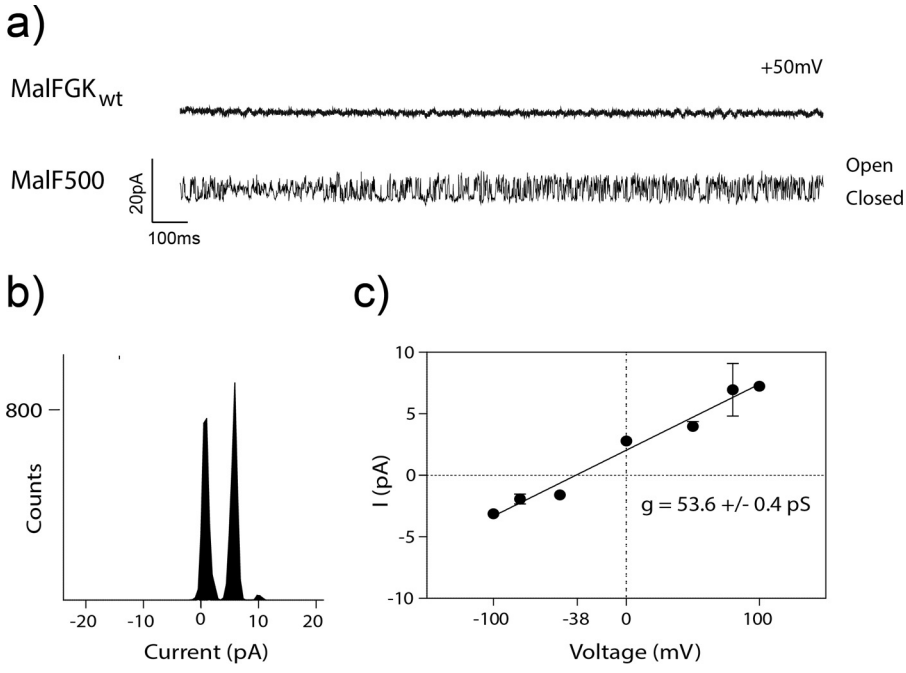

FIGURE 4. **Ion channel activity of MalF500 in planar lipid bilayers.** *a*, the electrical currents were recorded across a planar lipid bilayer (70% DOPC, 30% DOPG) at a holding membrane potential of +50 mV. Current traces were filtered at 500 Hz. The traces for the wild-type MalFGK$_2$ were recorded after >15 fusion events using nystatin/ergosterol as a reporter system indicating protein delivery. *b*, histogram of current amplitudes. The number of channel events obtained at +50 mV was determined using the Clampfit analysis program and the single channel search function. The currents were plotted as a function of their intensity. *c*, current-voltage curve for MalF500. Current amplitudes (*I (pA)*) were plotted according to the applied holding voltage. The slope of the curve represents the channel conductance in picosiemes. The reversal potential is −38 mV, as indicated by the x intercept of the curve.

insensitive given the linear voltage-current relationship, (ii) is anion-selective with a reversal potential (−38 mV) that is close to the calculated Nernst potential for chloride (−37 mV), and (iii) has rapid gating kinetics with an average dwell time for the opening state of only ~2–20 mS. Such quick opening and closing kinetics suggest that the transporter is conformationally flexible. This is in contrast to wild type MalFGK$_2$ which, throughout the experiment, remained stably closed (Fig. 4*a*).

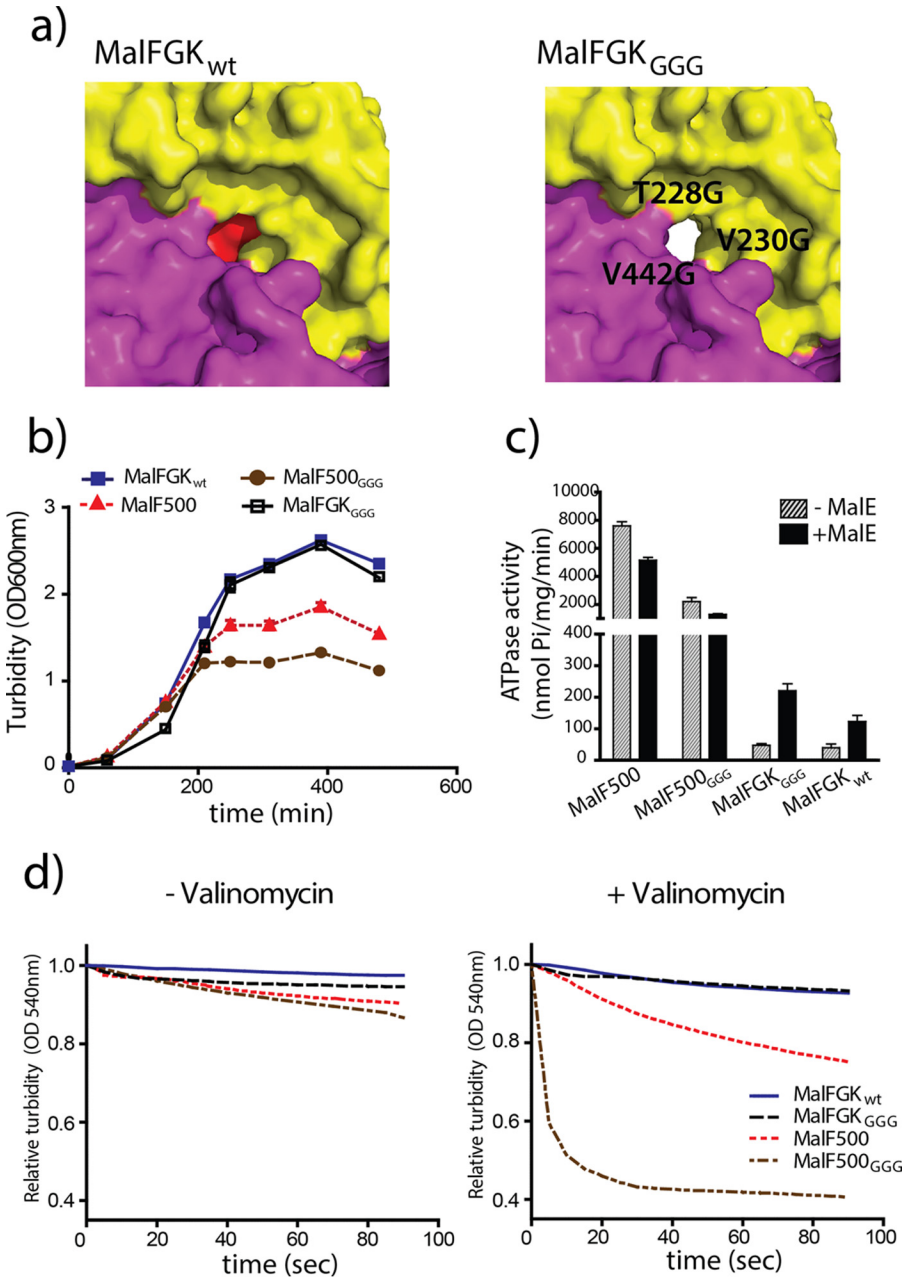

FIGURE 5. **The periplasmic gate seals MalF500.** *a*, the three gating residues (*red*, MalF$_{V442}$, MalG$_{T228}$, and MalG$_{V230}$) forming the periplasmic gate on MalF (*yellow*) and MalG (*pink*) were mutated to glycine residues. The space-filling representation was created with PyMOL using the inward-facing crystal structure of MalFGK$_2$ (PDB code 3FH6). *b*, growth curve of *E. coli* overproducing the indicated complex. Cells were grown in LB liquid medium at 37 °C for 150 min before induction with 0.2% arabinose. *c*, ATPase activity. Proteoliposomes containing the indicated mutant complex (0.5 μM) were incubated with maltose (1 mM) at 37 °C with or without MalE (1 μM) as indicated. Standard deviation was obtained from three separate experiments. *d*, spheroplast assays. Spheroplasts were diluted into an iso-osmotic solution of KCl in the presence or absence of valinomycin (15 μM). Cell lysis was monitored every 5 s at 540 nm.

Although bilayers often contained more than one channel, single-channel opening events were easily identified and used to calculate the ion conductance of MalF500. The histogram of current amplitudes and conductance magnitude were plotted as a current-voltage curve; the slope represents the single-channel conductance in picosiemens (Fig. 4*c*).

The Periplasmic Gate Seals Mal500—The resting maltose transporter (*i.e.* inward-facing) is sealed by gating loops on the periplasmic side of the membrane (6). The aminoacyl side chains MalF$_{V442}$, MalG$_{T228}$, and MalG$_{V230}$ form this interface (Fig. 5*a*). These residues were replaced by the short-chain amino acid glycine. According to the space-filling model (Fig. 5*a*), such mutations produce a wide-open pore in lieu of the gate. Surprisingly, results from the cell growth (Fig. 5*b*), ATPase activity (Fig. 5*c*), and cell membrane permeability assays (Fig. 5*d*) reveal that MalFGK$_{GGG}$ behaves much like the wild type. The glycine residues were then introduced into MalF500 to produce the mutant MalF500$_{GGG}$. In this case, we observed an immediate and strong growth defect upon protein production (Fig. 5*b*) together with a dramatic increase in cell membrane permeability (Fig. 5*d*). We note that the ATPase activity of MalF500$_{GGG}$ is ~4-fold less than that of MalF500 (Fig. 5*c*), sug-

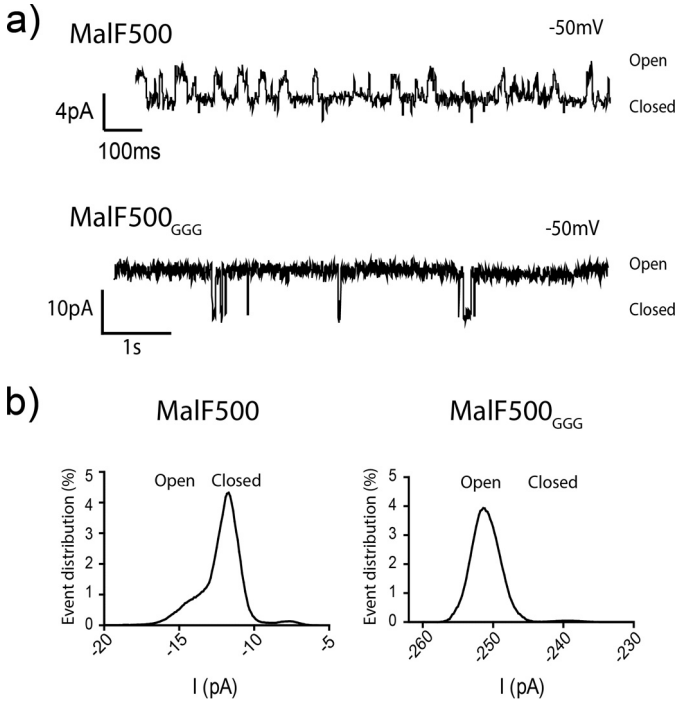

FIGURE 6. **Ion channel activity of MalF500$_{GGG}$.** *a*, typical electrical currents. Traces were obtained at a holding potential of −50 mV. *b*, all point histogram of current amplitudes. The number of channels present in the MalF500$_{GGG}$ bilayer (≈25 channels incorporated, −250 pA) results in a higher total current amplitude than observed for MalF500 (≈3 channels incorporated, −15 pA). For MalF500$_{GGG}$, the observed channels are predominantly open, therefore concurrent closing events are rare, and the all-point histogram shows only two current distributions despite the presence of multiple channels. The number of channels incorporated is determined by dividing the maximum observed current by the amplitude of one opening event, as observed in the traces represented in *a*.

gesting that ATP consumption is not the primary reason for the higher growth defect of MalF500$_{GGG}$. Apparently, the nature of the gating residues is particularly important when the transporter rests in a conformation near to the transition state.

MalF500$_{GGG}$ Forms a Quasi-permanently Open Membrane Channel—The mutant MalF500$_{GGG}$ was purified and inserted into planar lipid bilayers (Fig. 6*a*). In contrast to MalF500, which is equally distributed between open and closed states, MalF500$_{GGG}$ behaves like an open-state channel (Fig. 6*b*). The recordings (Fig. 6*a*) show that the frequency of a gating event is very slow (every ~1–2 s compared with ~20 ms for to MalF500). This increased open pore duration is consistent with both the dramatic increase in cell membrane permeability (Fig. 5*d*) and the very strong effect on bacterial growth (Fig. 5*b*). Single-channel recordings could not be captured with the MalF500$_{GGG}$ mutant; however, isolated closing events could be detected in bilayers containing multiple copies of the mutant (Fig. 6*a*). The rate of these closing events was such that only one channel of ~25 was observed closing at a time.

Discussion

The two major conformational states of the maltose transporter, inward-facing and outward-facing, appear sealed against ions and water molecules (6, 9, 32). However, whether the impermeability is maintained when the transporter cycles between these two states is unknown. These intermediate conformations are structurally difficult to characterize and, in the case of MalF500, also difficult to crystallize (19). Recent computer simulations suggest that water molecules can permeate through the substrate passageway when the transporter pass through intermediate conformations; however the pore is very narrow, and it is open for only a few nanoseconds (9).

Here we have augmented access to the intermediate conformations using the mutant MalF500, which carries the mutations MalF$_{G338R}$ and MalF$_{N505I}$. These mutations destabilize the inward-facing conformation, thereby decreasing the energy barrier for the transition (6, 20, 22). As a result, the MalF500 mutant is capable of spontaneously adopting the outward-facing conformation independently of ATP (Fig. 1). Through the use of this mutant, we show that increased access to the intermediate conformations allows a significant degree of ion conduction (Fig. 4). The currents measured are high ($>10^7$ ions/s), indicative of a movement of ions through a channel-like structure (12, 33). In addition, the frequency of channel closing and opening is very fast: every few milliseconds. This rapid cycling is consistent with the decreased energy barrier between the inward- and outward-facing conformations and with the exceptional ability of this mutant to hydrolyze a large amount of ATP. The results also show that mutations in MalF500 that stabilize its conformation, and therefore diminish its basal ATP activity, also diminish ion conduction (Fig. 3). Interestingly, the conductance and spheroplast assays indicate that MalF500 is selective for Cl^- over K^+, although there is no obvious structural characteristic in MalFGK$_2$ to explain this selectivity. Notwithstanding, our data show that MalFGK$_2$ must rest away from the conformations adopted by MalF500 to preserve the membrane barrier. This membrane barrier is particularly important in bacteria because ion gradients represent a main energy source (34). It is therefore not surprising that overproduction of MalF500, and especially MalF500$_{GGG}$, results in a significant bacterial growth defect (Fig. 5*b*). This growth defect may reflect the energetic cost associated with the use of counteracting pumps required to compensate for the leakage of chloride ions.

The periplasmic gate on MalFGK$_2$ is formed at the interface of four α helices (6). Surprisingly, we find that alteration of this interface (*i.e.* introduction of the mutations MalF$_{V442G}$, MalG$_{T228G}$, and MalG$_{V230G}$) does not alter the function of the gate: the mutant is viable and we do not detect increased ion conductance (Fig. 5*d*). This result was rather unexpected because a space-filling computer model suggests that the glycine residues leave an open pore over the transport pathway (Fig. 5*a*). It is therefore possible that an energetic pressure is forcing the mutated gate structure to adopt a conformation that recreates this essential membrane seal. This phenomenon has been reported in the case of the SecYEG translocon after the deletion of the plug domain (35). In contrast, introduction of the glycine residues into MalF500 leads to a quasi-permanently open pore (Fig. 6). The residues forming the periplasmic gate are therefore critical when the transporter rests in a conformation close to the transition state.

Active transporters and ion channels function by different mechanisms (10), but our results show that the maltose transporter can acquire a channel-like activity after just a few perti-

nently located mutations. In the case of CFTR, it is proposed that the stabilization of an intermediate conformation is at the origin of the conversion of this transporter into a chloride channel (36). Specifically, comparisons made with the closely related ABCA4 transporter suggest that the mutation of a salt bridge positioned far away from the gate region might have been crucial for conversion of the ancestral transporter into a channel-like state. After this initial conformational shift, the modern pore and gate regions in CFTR were acquired through additional mutations (36). Consistent with this hypothesis, our results reveal that a simple disruption to the gate region, as in the case of MalFGK$_{GGG}$, does not suffice to create an ion channel. It is rather the mutations that promote access of the transporter to intermediate conformations, like in MalF500, that are responsible for the ion channel activity.

Author Contributions—M. L. C., H. B., and F. D. conceived the study. M. C. designed, performed, and analyzed the experiments. M. L. C. and F. D. wrote the paper. All authors analyzed the results and approved the final version of the manuscript.

Acknowledgments—We thank Filip Van Petegem for access to the planar bilayer work station and members of our laboratory for critical reading of the manuscript.

References

1. Jardetzky, O. (1966) Simple allosteric model for membrane pumps. *Nature* **211,** 969–970
2. ter Beek, J., Guskov, A., and Slotboom, D. J. (2014) Structural diversity of ABC transporters. *J. Gen. Physiol.* **143,** 419–435
3. van der Does, C., and Tampé, R. (2004) How do ABC transporters drive transport? *Biol. Chem.* **385,** 927–933
4. Slotboom, D. J. (2014) Structural and mechanistic insights into prokaryotic energy-coupling factor transporters. *Nat. Rev. Microbiol.* **12,** 79–87
5. Li, J., Wen, P.-C., Moradi, M., and Tajkhorshid, E. (2015) Computational characterization of structural dynamics underlying function in active membrane transporters. *Curr. Opin. Struct. Biol.* **31,** 96–105
6. Khare, D., Oldham, M. L., Orelle, C., Davidson, A. L., and Chen, J. (2009) Alternating access in maltose transporter mediated by rigid-body rotations. *Mol. Cell* **33,** 528–536
7. Krishnamurthy, H., Piscitelli, C. L., and Gouaux, E. (2009) Unlocking the molecular secrets of sodium-coupled transporters. *Nature* **459,** 347–355
8. Forrest, L. R., and Rudnick, G. (2009) The rocking bundle: a mechanism for ion-coupled solute flux by symmetrical transporters. *Physiology* **24,** 377–386
9. Li, J., Shaikh, S. A., Enkavi, G., Wen, P.-C., Huang, Z., and Tajkhorshid, E. (2013) Transient formation of water-conducting states in membrane transporters. *Proc. Natl. Acad. Sci. U.S.A.* **110,** 7696–7701
10. Gadsby, D. C. (2009) Ion channels versus ion pumps: the principal difference, in principle. *Nat. Rev. Mol. Cell Biol.* **10,** 344–352
11. Kaback, H. R., Dunten, R., Frillingos, S., Venkatesan, P., Kwaw, I., Zhang, W., and Ermolova, N. (2007) Site-directed alkylation and the alternating access model for LacY. *Proc. Natl. Acad. Sci. U.S.A.* **104,** 491–494
12. DeFelice, L. J., and Goswami, T. (2007) Transporters as channels. *Annu. Rev. Physiol.* **69,** 87–112
13. MacAulay, N., Gether, U., Klaeke, D. A., and Zeuthen, T. (2002) Passive water and urea permeability of a human Na^+/glutamate cotransporter expressed in *Xenopus* oocytes. *J. Physiol.* **542,** 817–828
14. Duquette, P. P., Bissonnette, P., and Lapointe, J. (2001) Local osmotic gradients drive the water flux associated with Na^+/glucose cotransport. *Proc. Natl. Acad. Sci. U.S.A.* **98,** 3796–3801
15. Chen, T.-Y., and Hwang, T.-C. (2008) CLC-0 and CFTR: chloride channels evolved from transporters. *Physiol. Rev.* **88,** 351–387
16. Davidson, A. L., Dassa, E., Orelle, C., and Chen, J. (2008) Structure, function, and evolution of bacterial ATP-binding cassette systems. *Microbiol. Mol. Biol. Rev.* **72,** 317–364
17. Wen, P.-C., and Tajkhorshid, E. (2011) Conformational coupling of the nucleotide-binding and the transmembrane domains in ABC transporters. *Biophys. J.* **101,** 680–690
18. Bao, H., and Duong, F. (2014) Nucleotide-free MalK drives the transition of the maltose transporter to the inward-facing conformation. *J. Biol. Chem.* **289,** 9844–9851
19. Davidson, A. L. (2002) Mechanism of coupling of transport to hydrolysis in bacterial ATP-binding cassette transporters. *J. Bacteriol.* **184,** 1225–1233
20. Bao, H., Dalal, K., Wang, V., Rouiller, I., and Duong, F. (2013) The maltose ABC transporter: action of membrane lipids on the transporter stability, coupling and ATPase activity. *Biochim. Biophys. Acta.* **1828,** 1723–1730
21. Davidson, A. L., Shuman, H. A., and Nikaido, H. (1992) Mechanism of maltose transport in *Escherichia coli*: transmembrane signaling by periplasmic binding proteins. *Proc. Natl. Acad. Sci. U.S.A.* **89,** 2360–2364
22. Daus, M. L., Grote, M., and Schneider, E. (2009) The MalF P2 loop of the ATP-binding cassette transporter MalFGK2 from *Escherichia coli* and *Salmonella enterica* serovar Typhimurium interacts with maltose binding protein (MalE) throughout the catalytic cycle. *J. Bacteriol.* **191,** 754–761
23. Bao, H., and Duong, F. (2012) Discovery of an auto-regulation mechanism for the maltose ABC transporter MalFGK2. *PLoS ONE* **7,** e34836
24. Klock, H. E., and Lesley, S. A. (2009) In *Methods in Molecular Biology* (Doyle, S. A., ed.), pp. 91–103, Humana Press, Totowa, NJ
25. Maillard, A. P., Lalani, S., Silva, F., Belin, D., and Duong, F. (2007) Deregulation of the SecYEG translocation channel upon removal of the plug domain. *J. Biol. Chem.* **282,** 1281–1287
26. Woodbury, D. J., and Miller, C. (1990) Nystatin-induced liposome fusion: a versatile approach to ion channel reconstitution into planar bilayers. *Biophys. J.* **58,** 833–839
27. Lanzetta, P. A., Alvarez, L. J., Reinach, P. S., and Candia, O. A. (1979) An improved assay for nanomole amounts of inorganic phosphate. *Anal. Biochem.* **100,** 95–97
28. Bradford, M. (1976) A rapid and sensitive method for the quantitation of microgram quantities of protein utilizing the principle of protein-dye binding. *Anal. Biochem.* **72,** 248–254
29. Bao, H., and Duong, F. (2013) ATP alone triggers the outward facing conformation of the maltose ATP-binding cassette transporter. *J. Biol. Chem.* **288,** 3439–3448
30. Covitz, K. M., Panagiotidis, C. H., Hor, L. I., Reyes, M., Treptow, N. A., and Shuman, H. A. (1994) Mutations that alter the transmembrane signalling pathway in an ATP binding cassette (ABC) transporter. *EMBO J.* **13,** 1752–1759
31. Park, E., and Rapoport, T. A. (2011) Preserving the membrane barrier for small molecules during bacterial protein translocation. *Nature* **473,** 239–242
32. Oldham, M. L., Khare, D., Quiocho, F. A., Davidson, A. L., and Chen, J. (2007) Crystal structure of a catalytic intermediate of the maltose transporter. *Nature* **450,** 515–521
33. Jayaram, H., Accardi, A., Wu, F., Williams, C., and Miller, C. (2008) Ion permeation through a Cl^- selective channel designed from a CLC Cl^-H^+ exchanger. *Proc. Natl. Acad. Sci. U.S.A.* **105,** 111940–111199
34. Maloney, P. C., Kashket, E. R., and Wilson, T. H. (1974) A protonmotive force drives ATP synthesis in bacteria. *Proc. Natl. Acad. Sci. U.S.A.* **71,** 3896–3900
35. Li, W., Schulman, S., Boyd, D., Erlandson, K., Beckwith, J., and Rapoport, T. A. (2007) The plug domain of the SecY protein stabilizes the closed state of the translocation channel and maintains a membrane seal. *Mol. Cell* **26,** 511–521
36. Jordan, I. K., Kota, K. C., Cui, G., Thompson, C. H., and McCarty, N. A. (2008) Evolutionary and functional divergence between the cystic fibrosis transmembrane conductance regulator and related ATP-binding cassette transporters. *Proc. Natl. Acad. Sci. U.S.A.* **105,** 18865–18870